Icarus 340 (2020) 113608

Contents lists available at ScienceDirect

Icarus

journal homepage: www.elsevier.com/locate/icarus

Multistage ice-damming of volcanic flows and fluvial systems in Northeast Syrtis Major

Connor Matherne [a,*], J.R. Skok [a,b], J.F. Mustard [c], Suniti Karunatillake [a], Peter Doran [a]

[a] Department of Geology and Geophysics, Louisiana State University, United States of America
[b] SETI Institute, United States of America
[c] Department of Geological Sciences, Brown University, United States of America

ARTICLE INFO

Keywords:
Mars Hesperian glaciation
Northeast Syrtis Major
Ice sheet
Basin
Channel

ABSTRACT

The northeast edge of the Syrtis Major volcanic complex records a diverse history of volcanism and climate of early Mars which has long been argued to be dominated by icy or wet conditions. This region contains a stratigraphic record that spans the period of phyllosilicate secondary mineralogy from moderate pH alteration of the Early Noachian crust, to the more acidic, sulfate-forming, Hesperian period dominated by the adjacent volcanic plains of Syrtis Major Planum. A paleo-fluvial basin and channel system etched in the Syrtis Major volcanics is identified and analyzed using multiple instruments onboard the Mars Reconnaissance Orbiter. These observations and analysis link the current landscape and the basin's existence at the base of the Syrtis Major lava flow to a paleo-glaciation within the Isidis Basin. This paleo-glaciation formed ice sheets kilometers thick and ranged over hundreds of kilometers laterally and is responsible for halting the Syrtis Major flows in the Northeast Syrtis area to form the observed steep cliffs and the topographically flat mesa. Following this large scale glaciation, channels fed primarily by precipitation were etched into the Hesperian volcanics before filling the basin and flowing out an area of higher topography than is currently available due to the existence of an episodic ice dam before terminating in a potential, highly eroded, fan. The dynamic relationship between the climate and landscape evolution has left an imprint on the local geologic record of this complex region of Mars, with testable observations that could be made with the Mars 2020 Rover in the form of a highly jointed surface formed from lava ice interactions on the cliff face of the volcanic mesa.

1. Introduction

The northeast edge of the Syrtis Major complex is located on the western edge of the Isidis Basin (Fig. 1) and contains a basin and channel system with many morphological features and geologic units that have been suggested to be related to a global ocean or regional ice sheet during the Hesperian (Bramble et al., 2017; Guidat et al., 2015; Quinn and Ehlmann, 2019). This area straddles the geologic boundary between the Noachian, clay-rich crustal exposures of Nili Fossae (Ehlmann et al., 2009; Mustard et al., 2009) and the Hesperian volcanics of Syrtis Major (Fawdon, 2016; Hiesinger and Head, 2004). This global stratigraphic boundary is suggested to mark a global change in volcanic, fluvial and alteration activity (Bibring et al., 2006). The diversity of geologic processes and mineralogical units represented in the region makes it a complex but important region to understand. The oldest preserved local unit is the phyllosilicate-bearing Noachian crustal bedrock that forms the modern plains to the north of Syrtis Major. The region was then shaped and excavated during the formation of the Isidis impact basin at ~3.96 Ga (Werner, 2008) (Fig. 2). The basin formation created the regional slopes and topography that influences later fluvial processes. Olivine-bearing [$(Mg,Fe)_2SiO_4$] units were then emplaced throughout the region stratigraphically above the altered bedrock. Emplacement has been suggested as either impact melts from the Isidis event (Mustard et al., 2007), picritic lava flows (Tornabene et al., 2008), or more recent work suggesting they are emplaced through detrital sedimentation due to their association with topographic lows (Rogers et al., 2018). This was followed by the tectonic formation of the Nili Fossae troughs (Wichman and Schultz, 2008) cross-cutting the olivine-bearing units (Mustard et al., 2007, 2009). The region was subsequently shaped by the impact that formed Jezero crater. Subsequent fluvial activity formed the Jezero crater lake and deposited phyllosilicate-bearing deltas 3.74 Ga ago (Ehlmann et al., 2008a; Fassett and Head, 2005; Goudge et al., 2015;

* Corresponding author.
E-mail address: cmath31@lsu.edu (C. Matherne).

https://doi.org/10.1016/j.icarus.2019.113608
Received 20 July 2019; Received in revised form 29 November 2019; Accepted 18 December 2019
Available online 7 January 2020

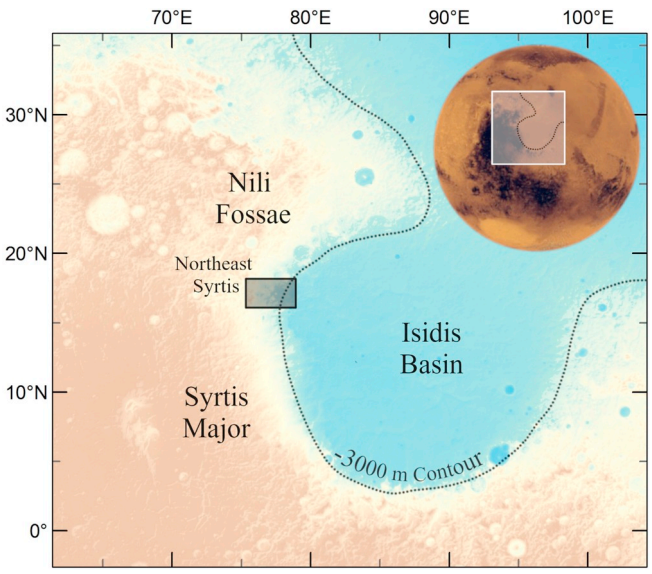

Fig. 1. The regional context of Northeast Syrtis on shaded MOLA map. The study area (dark shaded box on map, subsequently Fig. 3) is located at the junction of the early Hesperian, Syrtis Major volcanic flows, the Isidis Basin, and the Noachian clay-rich crustal exposures of Nili Fossae. Viking image of Mars is located in the upper right portion with a white box to show the location of the underlying image (Mars globe: NASA/USGS/ESA/DLR/FU Berlin (G. Neukum)).

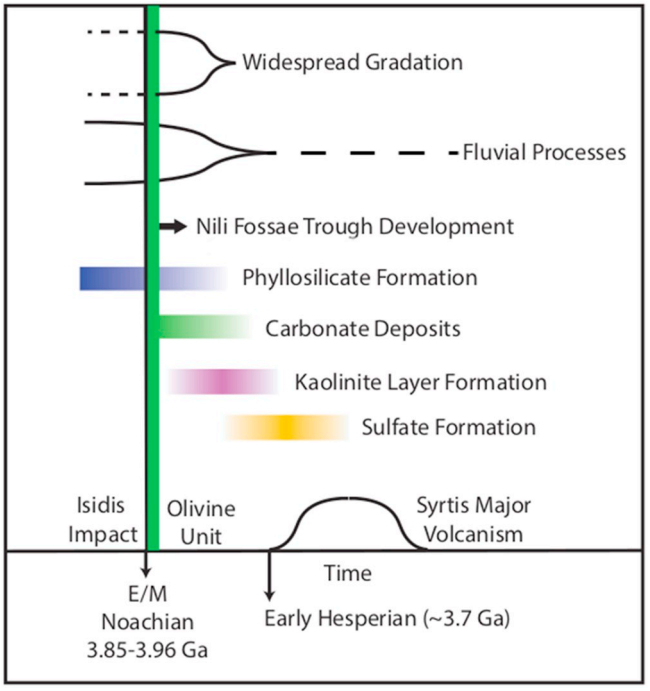

Fig. 2. The proposed timeline of regional geology in Northeast Syrtis. Regional gradation, fluvial processes, and phyllosilicate development would begin in the early Noachian. The regional topography was then created by an impact that created the Isidis Basin. This impact also deposited a regional olivine deposit that would be the catalyst for subsequent carbonate development. Further alteration in the bedrock lead to kaolinite development. Changes in global climate led to sulfate alteration and deposition. These units were then capped by Syrtis Major volcanism in the Early Hesperian before being eroded by later fluvial processes. Modified from Mustard et al., 2009.

Schon et al., 2012). The regional olivine-bearing unit was partially altered to a magnesium carbonate-bearing ($MgCO_3$) assemblage (Ehlmann et al., 2008b) and extensive surface leaching occurred in the altered basement units to create zones of kaolinite [$Al_2Si_2O_5(OH)_4$]. Stratigraphically above those units is a sulfate-bearing layer capped by the low viscosity, basaltic Syrtis Major volcanic flows (Bandfield et al., 2000; Ehlmann and Mustard, 2012; Simpson et al., 1982). How the sulfate unit formed is still debated, but recent work suggests a regional ground water system (Andrews-Hanna and Lewis, 2011) or regional Isidis ice sheet (Souček et al., 2015) would be required to explain the depositional history and further fracturing alteration of the unit (Quinn and Ehlmann, 2019).

The last major unit to be emplaced in the region was the Syrtis Major volcanic lavas that cap the local stratigraphy to the immediate southwest of our study region (Fawdon, 2016; Hiesinger and Head, 2004; Schaber, 2008). The study of Syrtis Major's eastern cliff forming morphology and the knobby terrain transition from Syrtis Major to the Vastitas Borealis unit of the Northern Lowlands suggests that the lavas may have encountered a volatile rich unit, such as an ice sheet (Edwards et al., 2013; Ivanov and Head, 2003). In addition to this, it is noted that lava flow margins are very irregular with steep cliffs that indicate possible lava-ice interactions (Ivanov and Head, 2003). The presence of ice deposits at mid-latitudes is predicted at times of high obliquity (Mustard et al., 2001) during the recent Amazonian and may be more likely during an earlier, more volatile-rich period in Martian history with evidence for Hesperian aged glaciation near the dichotomy in other parts of Mars (Davila et al., 2013).

The geologic complexity of the transition and its surface visibility motivate our investigation to constrain the local, late stage fluvial history of Northeast Syrtis. The emplacement of the Syrtis volcanics was followed by a period of fluvial erosional activity as noted by Mangold et al. (2008), who described the presence of a channel etched elsewhere into the Syrtis basalts. That channel and several related nearby fluvial features would have required a significant source of water to create the observed morphology within the basalts, with 515 km^3 of water estimated to form the fracturing and expansiveness of the sulfates within the area (Quinn and Ehlmann, 2019). We expand on the work by Mangold et al. (2008) by investigating a set of Hesperian-aged geomorphologic features that are similar, but are instead located on the transition from the Hesperian volcanics to the adjacent Noachian terrains. We complement prior works by Bramble et al. (2017) who characterized the morphology of the geologic units, and several others who have provided spectral analysis (Ehlmann et al., 2008b; Goudge et al., 2015; Mustard et al., 2009), by focusing our analysis on the sedimentological units following a tentative gravitational equipotential surface within the basin, such as a magnesium carbonate layer and volcanic units tracing the topography contours within the basin.

We respond to key questions motivated by the basinal landscape. First: what are the likeliest hydrological sources for the upland source channels? Second: what terminated a large volcanic flow to preserve an isolated basin? Third: what enabled basin drainage via topographically higher outlet channels, despite the existence of a topographically lower potential outlet to the SE? Once addressed, we look to answer the overarching question: to what extent do the findings suggest glacial activity at this geologic transition zone?

1.1. *Local fluvial system features*

The Northeast Syrtis region's fluvial morphology can be divided into two main periods. The first period is defined by the meandering rivers (Schon et al., 2012) and the delta formation in the Jezero Crater open basin lake (Ehlmann et al., 2008a; Fassett and Head, 2005), dated at 3.74 Ga (Fassett and Head, 2008), and pre-dates the Hesperian-aged volcanics that embay the lacustrine deposits (Goudge et al., 2012). The second period post-dates the Hesperian volcanics of Syrtis Major, with sources within the volcanic terrains as we explore here. Given those

two episodes of fluvial processes, we subdivide the region of interest into upland source channels, basin, outlet channel, and channel fan (Fig. 3). Current literature has mentioned the existence of the upland source channels (Hiesinger and Head, 2004), the basin (Bramble et al., 2017), and the outlet channels (Quinn and Ehlmann, 2019), however, the channel termination remains unaddressed in the literature.

1.1.1. Upland source channels

A morphologically subdued system of upland channels is apparent on top of a volcanic plateau emplaced in the early Hesperian (Fawdon et al., 2019; Hiesinger and Head, 2004) (Fig. 4). The braided, shallow channels start in the west and follow a shallowly dipping, 7 km wide basaltic plateau that previously floored a topographic low in the Noachian-aged material (Fig. 4A). In extending beyond the basaltic unit, the channels cross a few kilometer long flat-topped volcanic mesa (Fig. 4B) with cliffs over 100 m in height (Fig. 4E). On the mesa, the channels spread predominantly to the east and the south, along with several minor extensions in different directions. The southern channel (Fig. 4D) leads to a closed basin immediately south of this plateau. The eastern channel system (Fig. 4C) continues off the volcanic plateau and erodes a channel that leads to the basin.

1.1.2. Basin

The eastern channel mentioned above leads directly to a topographic basin centered at 17.6°N 76.6°E (Fig. 5). The basin depression is ellipsoidal with an elongate southeast-northwest axis. The basin contains two potential outlet paths, one to the east, and one to the southeast. The southeast outlet is floored by loose particulate material that has been derived from adjacent cliff forming volcanics (Bramble et al., 2017). A lake would be required to have filled this basin in order to activate these outlet channels (Quinn and Ehlmann, 2019).

1.1.3. Outlet channels and termination

The basin has an outlet channel system on its eastern edge, with no outlet channels observed in the southeastern passage (Quinn and Ehlmann, 2019). The outlet channel erodes through the Noachian terrain for 48 km before terminating at an elevation of −3050 m in the modern MOLA topography at the edge of the Isidis Basin (Fig. 6).

2. Methods

Surface morphology was assessed using ~6 m/pixel images from the Context Camera (CTX) instrument on the Mars Reconnaissance Orbiter (MRO) spacecraft (Malin et al., 2007). Detailed morphology was also investigated using ~0.25 m/pixel images from the High Resolution Imaging Science Experiment (HiRISE) instrument on MRO (McEwen et al., 2007) where available. We maintain all imaging data in an ArcMap GIS database (Table 1). Topographic information and regional slope was determined using transects with Mars Orbiter Laser Altimeter (MOLA) gridded topography with a resolution of ~463 m/pixel or 128 pixels per degree (Zuber, 1992), and High Resolution Stereo Camera (HRSC) (Neukum and Jaumann, 2004) Digital Elevation Models (DEM). Local topography has been determined with CTX derived DEM. CTX DEMs were produced with the NASA Ames Stereo Pipeline software (Edwards and Broxton, 2012) or provided by the USGS Astrogeology Science Center using a blend of MOLA and HRSC images allowing for vertical accuracy as fine as 10 m (Fergason et al., 2018). A normalized and seamless mosaic was provided for the area by the Bruce Murray Laboratory for Planetary Visualization (Dickson et al., 2018). Channel branching angle is determined using CTX and HiRISE images by dividing up the channels into stream segments and finding the junction angle between these two segments (Seybold et al., 2017).

Mineral composition was determined with reflectance spectra by the Compact Reconnaissance Imaging Spectrometer for Mars (CRISM), a visible and near-infrared (VNIR) hyperspectral imaging instrument (Murchie et al., 2007). CRISM acquires full resolution targeted (FRT) images at 18 m per pixel spatial resolution and 544 spectral bands ranging from 0.36–3.9 μm (Murchie et al., 2007). CRISM images were calibrated with a volcano scan method (McGuire et al., 2009) to eliminate atmospheric effects and ratioed against spectrally bland areas covered by dust of average albedo and illumination within the image to improve detection of minerals with absorption bands that lie within spectral bands ranging from 1.9–2.1 μm. Table 1 lists examples of image and spectral data that we used.

Ages of the volcanic capping units were determined using CraterStats 2 within ArcMap using CTX images for the Syrtis Major volcanic unit to the west and two capping units within the basin (Fig. 9). Other areas within and around the basin were not counted due to low crater retention, stemming from their friability which is up to 78% lower than the volcanic units chosen (Palumbo and Head, 2018). Following the guideline of at least three orders of magnitude larger area than the smallest diameters for the craters, while maintaining crater diameters to be larger than 100 m, was implemented to avoid large uncertainties (Hartmann, 2005). However, it should still be noted that crater counted areas within the basin are <100 km^2 and are likely to be impacted by resurfacing events with associated high uncertainties (Warner et al., 2015). No secondary craters were observed within our units, a major critique of the crater counting method when using smaller craters as noted by McEwen et al. (2005).

3. Results

3.1. Upland source channels

The braided upland source channels etch the volcanic landscape with a diffuse origin. The channels bifurcate at twenty different locations at an average angle of 43° ± 21° as they move down the volcanic slope before dispersing into multiple paths on the volcanic mesa. The channels

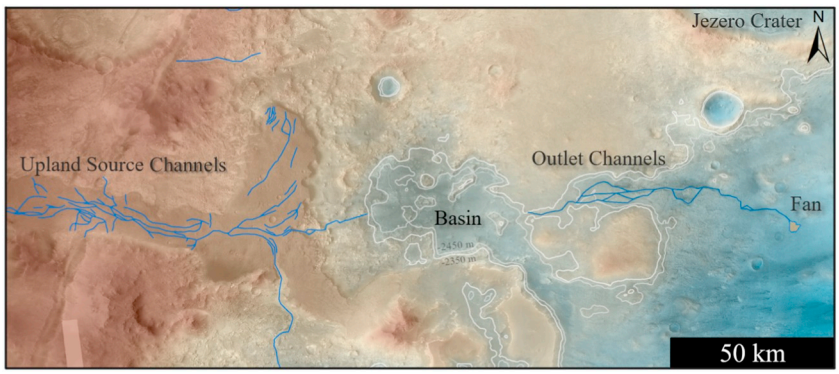

Fig. 3. CTX mosaic, with colored HRSC DEM overlay of the channel system on the edge of Northeast Syrtis with Jezero Crater labeled for orientation.

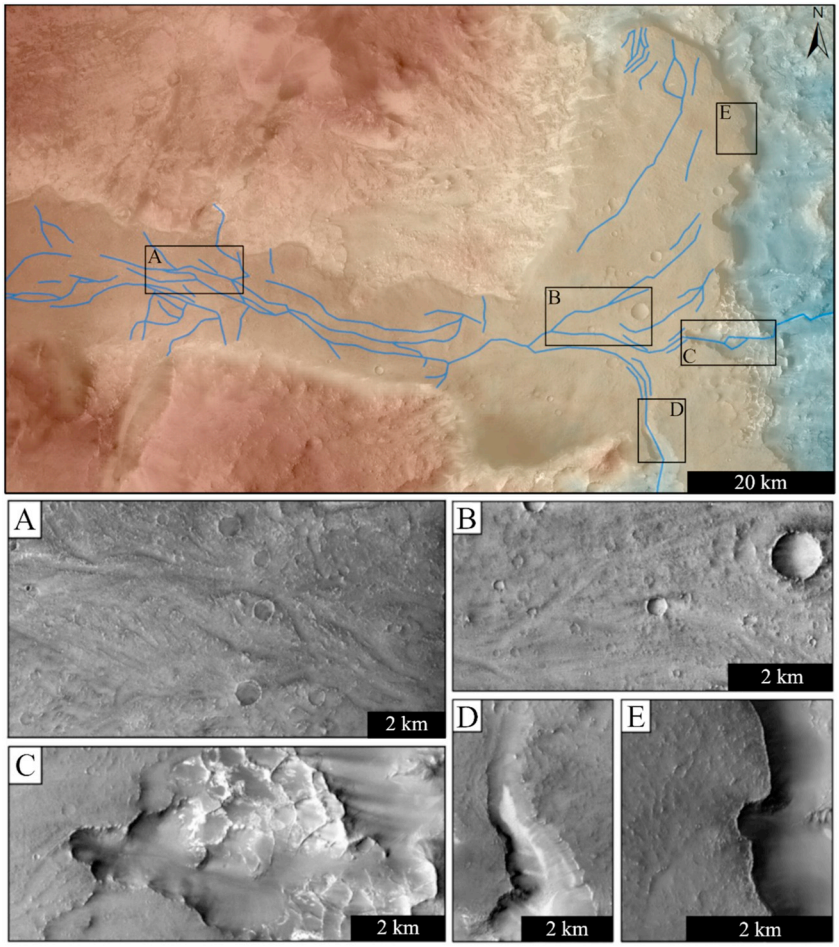

Fig. 4. Upland source channel terrain. Top panel is a CTX mosaic with shaded relief HRSC DEM overlay. A) Braided erosional grooves on the slightly down sloping volcanic plane. B) CTX mosaic shows flow features that eroded the igneous rock layer along the topographically flat volcanic mesa. The positive relief remnants of erosion, such as around the crater near center are morphologically consistent with flow in the direction of the current slope. These flow features spread primarily eastward and southward, eventually converging into two tens-of-meter wide channels. A smaller number of erosional features are identifiable in a northerly direction. C) Light-toned sulfate bearing material with boxwork texture with the basin inlet channel eroding the Syrtis Major volcanics. D) Southern channel eroding into the Syrtis Major volcanics E) Highly irregular boundary of the volcanic flows with steep cliffs over 100 m high.

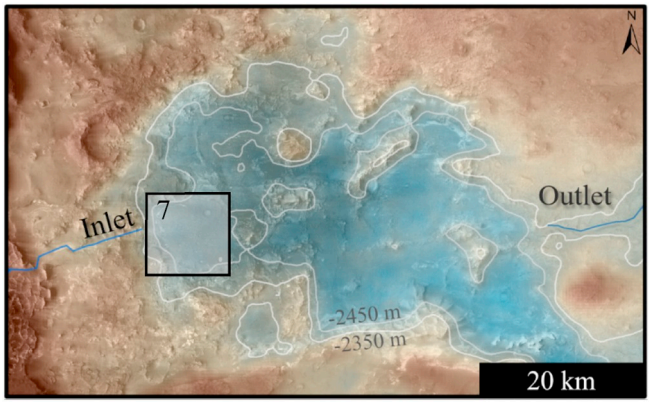

Fig. 5. CTX mosaic with colored HRSC DEM overlay shows a topographic low that forms the basin of the purported past fluvial system. The exterior contour (−2350 m) shows the topographic boundary that would have activated the eastern outlet channel. Shaded box shows location of Fig. 7.

exit the mesa by diverting to two different areas: one into the basin to the east, the other off the mesa to the south. The major system that is directed south erodes back the mesa 4.2 km (Fig. 4D), and ends in the poorly preserved remnants of a possible sediment fan roughly 20 km from the mesa. The other system trends eastward off of the mesa, eroding it back a distance of 3.5 km (Fig. 4C). The channel continues easterly as it encounters a boxwork texture of light-toned sulfate bearing material (Quinn and Ehlmann, 2019) before entering the basin (Fig. 4C).

3.2. Basin

Current topography shows that the basin would drain via a 3 km wide gap to the southeast if filled above the −2450 m, 100 m lower than the water height that would have activated the outlet channel to the east (Fig. 5). However, we find no major indications of fluvial morphology or modification to suggest runoff in the southeastern gap. While this gap is floored by loose material that may obscure any of these features, we do not observe any of these features emerging once the loose material has lessened. At times when discharge was occurring only through the northeastern outlet channel, the lake would cover approximately 300 km^2 with a maximum depth of 200 m. Along the eastern side of the basin, light-toned, spectrally-dominated magnesium carbonate layer based on CRISM observations can be seen tracing the topography in the area and is exposed in the rims of nearby impacts (Fig. 7).

3.3. Outlet channels

The proposed lake inside the basin would have emptied through an outlet channel that drained east, carving through the Noachian clay-bearing crust (Fig. 6). This channel can be traced for 48 km as it drops ~750 m from an elevation of −2330 m at the basin rim to −3050 m elevation eastward. The channel begins with a well-defined and preserved path and a width of ~500 m. After the first ~7 km, the channel morphology becomes complex with signs of braiding or multiple channel forming episodes. One section, 10 to 25 km from the head, contains a branching path that contains at least four distinct sub-channels. The channel also bifurcates 30 to 35 km from the head. In addition, from the start at the basin, there are two potential topographic channels. Using

Fig. 6. Mapped outlet channels. Topography shows multiple eroded channels flowing from west to east before terminating in a fan. Four visually distinct and two additional potential channels derived from topography could have been active during different fluvial episodes as evident in the DEM overlay.

Table 1
Targets, image IDs, instruments, and associated figures for each image used.

Target	Image ID	Instrument	Figure
Study Area Mosaic	E72_N16	CTX	3, 4
Study Area Mosaic	E76_N16	CTX	3, 4, 5, 6, 9
Proposed Fan	ESP_036407_1975_RED	HiRISE	8A, 8B
Sagan Crater Fan	B21_018003_1916_XN_11N030W	CTX	8C
Libya Montes Fan	D05_029260_1828_XN_02N274W.tiff	CTX	8D
Basin CRISM	FRT000199C7	CRISM	7C
Basin HiRISE	ESP_04882_1980_RED	HiRISE	7A, 7B

the combined visual and topographic mapping, we can identify at least six variations in the outlet path. Sections of the channel are subdued, but a majority are well defined with sharp sides. Much of the length of the channel floor now has aeolian ripples that are consistently perpendicular to the channel walls, indicating a localized wind regime parallel to channel walls, before terminating.

3.4. Outlet channel termination

The channel terminates at −3050 m and forms a heavily dissected fan (Fig. 8) that covers an area of 2.1 km^2. The fan does not show significant topography beyond the regional slope. About 12.5 km downslope from the fan, two additional channel fragments, 4 km in length and morphologically similar to the outlet channel (in terms of width, depth, and sinuosity), are separated by basin floor material. Due to the friability of the local geology and the size of the fan, we are unable to determine the fan age using crater counting methods.

3.5. Dating of the volcanic units

The Hesperian Syrtis Major Volcanics were crater counted to an age of 3.4 ± 0.05 Ga using 170 craters within the area (Fig. 9A). The dark crater retaining unit (Bramble et al., 2017) within the basin was dated to 2.1 ± 0.2 Ga for the eastern unit using 97 craters (Fig. 9B). The western unit within the basin was dated to the same age of 2.1 ± 0.2 Ga using 99 craters. While the dark crater retaining units within the basin correspond in age, the reader should note that due to the size of these units and the susceptibility to resurfacing events, they do contain large uncertainties compared relatively to the Hesperian Syrtis Major Volcanics to the west.

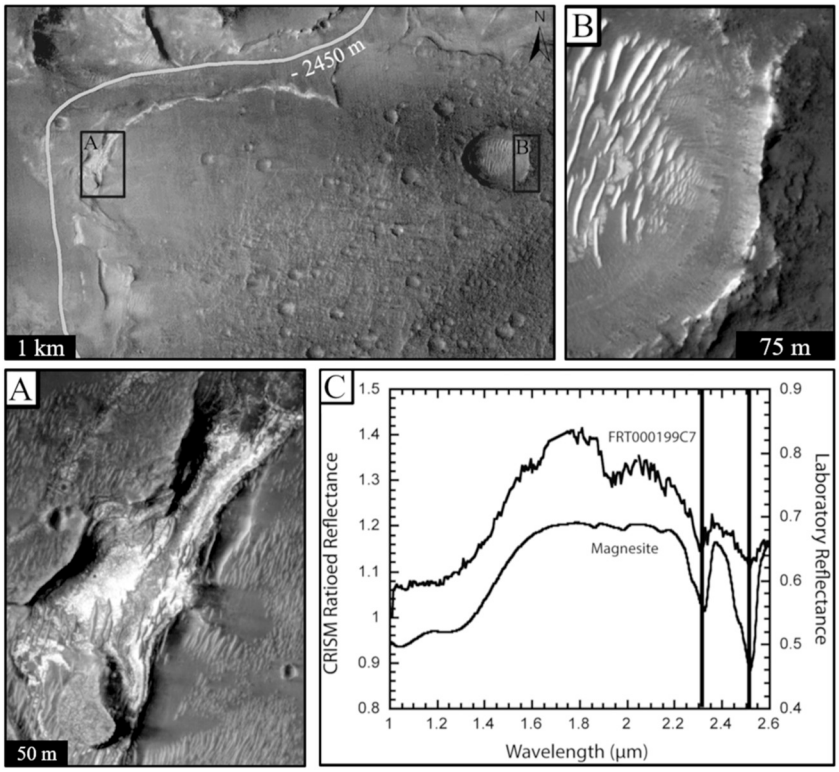

Fig. 7. CTX view of basin fill unit. The unit is highly textured and retains craters. The fill unit is spectrally bland. A) The fill unit is surrounded by light-toned, layered olivine and magnesium carbonate deposits that trace the topography of the area shown in this HiRISE image. B) HiRISE view showing the carbonates underlying the fill unit and exposed around the edges of a 500 m crater on the basin fill, constraining the fill unit thickness to ~40 m. C) CRISM ratioed reflectance of magnesium carbonate ($MgCO_3$) on edge of basin fill units. (FRT000199C7). Laboratory magnesite spectra for comparison (RELAB: LACB03B). Characteristic absorption features marked with vertical lines at 2.32 and 2.51 μm for magnesium carbonate (Ehlmann et al., 2008b).

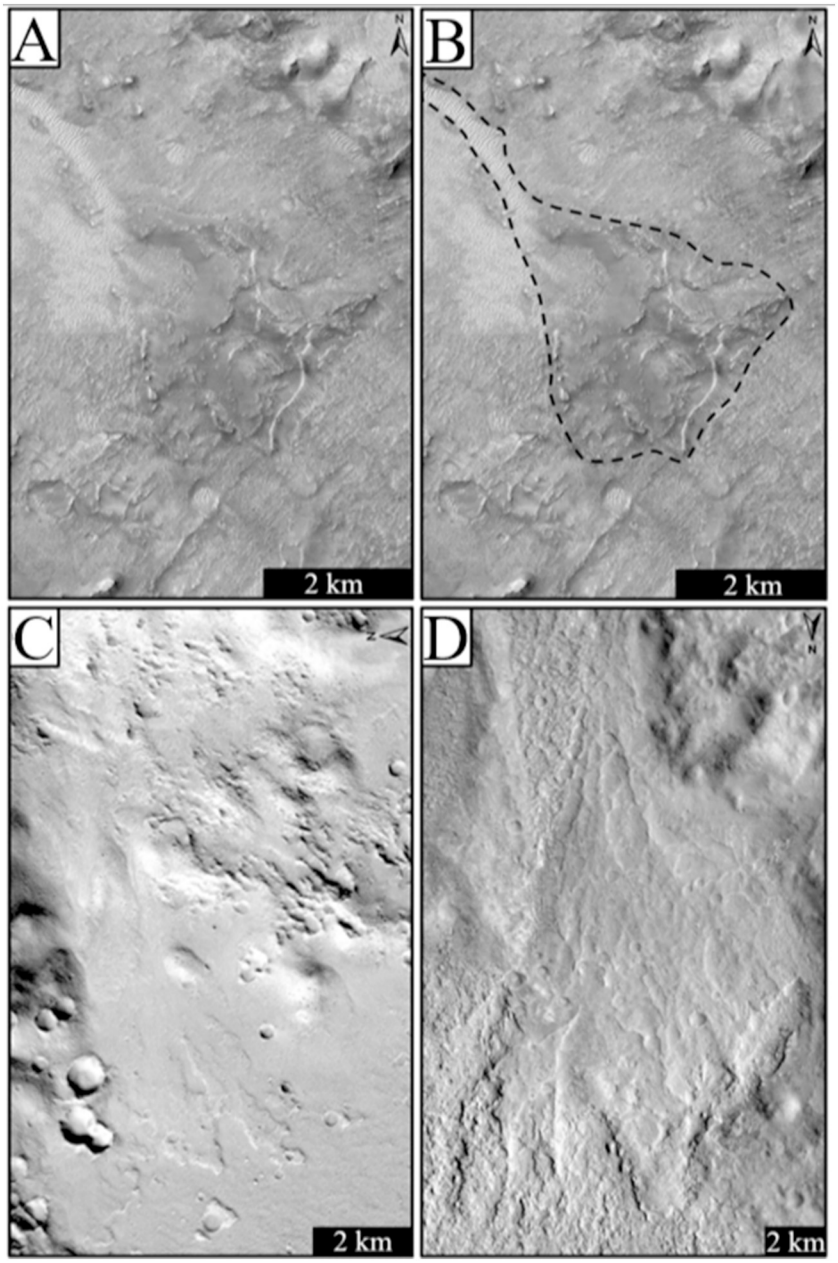

Fig. 8. A) HiRISE image of the outlet channel that leads to a deeply eroded, 2.1 km^2 fan at an elevation of −3050 m. B) Fan and channel outlined in a black dashed line for ease of identification. C) CTX image of a highly eroded fan located within Sagan Crater (Salese et al., 2019) D) CTX image of a highly eroded delta located in Libya Montes (Erkeling et al., 2012). Both C and D are included as references to other highly eroded fans of similar size and shape.

3.6. Critical thickness of Syrtis Major volcanic flows

Two major characteristics of the Syrtis Major volcanic flows of interest are the critical thickness and the height of the cliffs that these flows formed along the topographic mesa. The difference between these two heights is crucial for determining if the flow should have continued along its path, or if it encountered an obstruction. The critical thickness is calculated using the standard equation $h = \frac{S_y}{g\rho \tan\alpha}$, where S_y is lava yield strength, g is gravity, ρ is density and α is the angle of the slope (Rothery et al., 2018). In order to derive probable critical thicknesses, we use a value of 3.72 m/s^2 for g corresponding to Mars's gravity (Hirt et al., 2012), ρ of 3000 kg/m^3 representing standard basaltic composition (Stolper and Walker, 1980), and a regional slope of 12°. The lava yield strength parameter is varied in order to yield the widest range of possible thickness by using a minimum from Mauna Loa, Hawaii of 3.5 × 10^2 Pa, and maximum from Ascraeus Mons of 8.3 × 10^4 (Wilson and Head, 1994). Those returns values of 0.15 m and 35 m respectively for the critical thickness. The cliffs on the volcanic mesa are consistently over 100 m in height, with the northeastern side containing the largest cliffs at over 200 m high.

4. Discussion

Having described each of the components of this basin system separately, we now integrate these observations to interpret the underlying geologic processes. By assessing each question, its importance, and offering potential hypotheses to explain the observations, before finally addressing their individual significance to glacial activity throughout the study region.

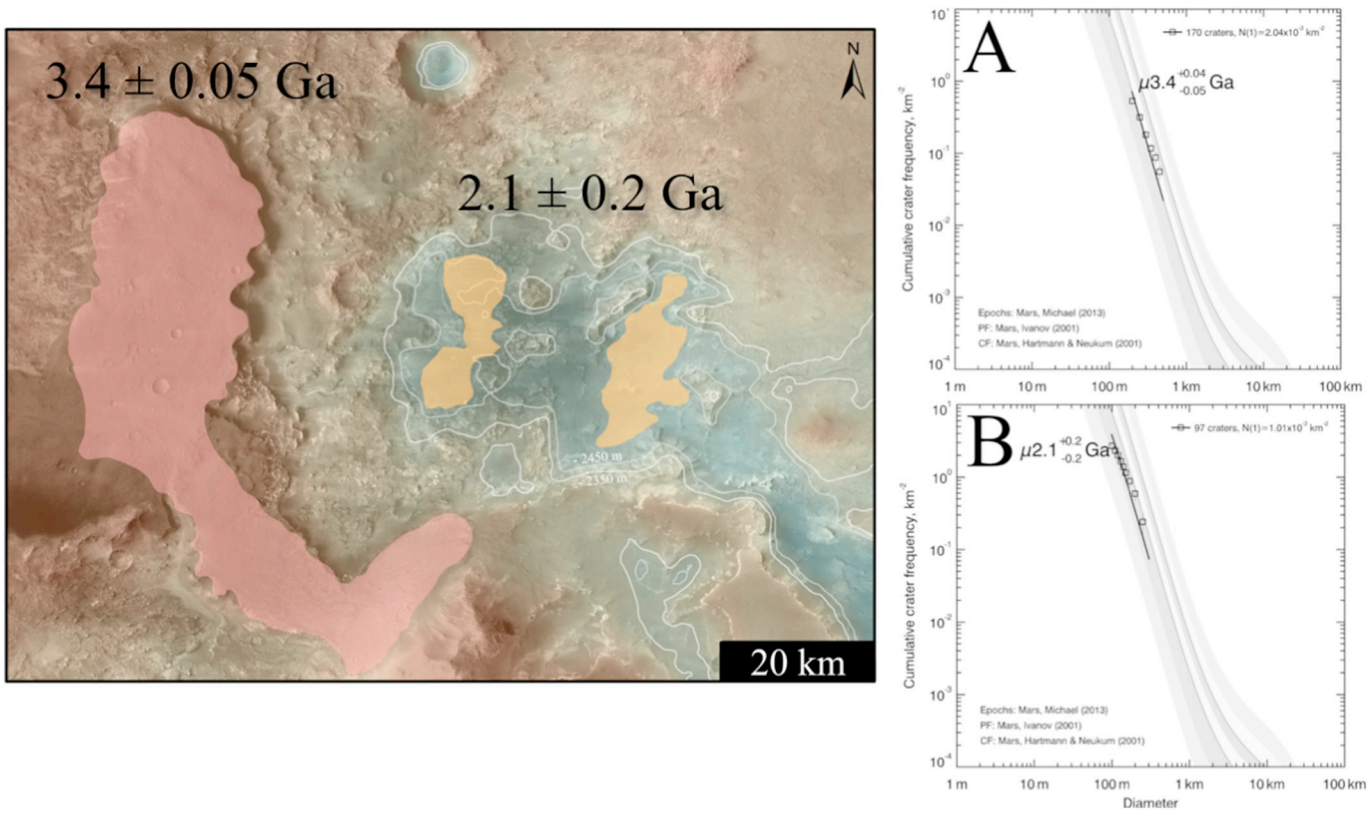

Fig. 9. CTX mosaic shows the three regions which were crater counted relative to their position in the basin. Two areas within the basin (yellow) were dated to the Amazonian while the larger unit to the west (pink) is dated to the Hesperian. A) Age determination for the delineated pink region B) Age determination for the eastern yellow unit within the basin. The western unit shows a similar age to (B) with an equal number of craters, calculated age, and size to the eastern unit. Plots for both A and B were created using Craterstats 2.0 (Hartmann, 2005). (For interpretation of the references to colour in this figure legend, the reader is referred to the web version of this article.)

4.1. Q1: What are the likeliest hydrological sources for the upland source channels?

We observe that the upland channels lack a clear origin point, and in Fig. 4A the channels bifurcate and etch through the volcanic cap rock until they erode back the edge of the volcanic plateau (Fig. 4D, E). Of those, only the most eastwardly channel connects to the basin via surface morphology while the others head to parts of the surrounding terrain, with laterally fading geomorphic expression. While a fluvial origin has been favored, alternative mechanisms have been considered, including effusive lava channels. However, the lack of a spatially localized source, the meanders, lack of a debris field, and the erosion at the edge of the plateau are collectively more consistent with fluvial erosion rather than a lava channel formation (Crown and Ramsey, 2017; Susko et al., 2017).

Groundwater sapping was also considered as a source of the channels given the existence of other groundwater systems south of this area (Mangold et al., 2008). However, this area is topographically higher by over 1 km than estimated groundwater depth for the relevant time period (Salese et al., 2019). Water can flow upwards to the surface through confinement within dikes (Salese et al., 2019). Extensive dike formations associated with both Syrtis Major and the Isidis Basin could possibly displace the groundwater table this way. However, we do not see morphology consistent with groundwater sapping, such as fissures, or stepped deltas. In addition, a dike-controlled water table would require elevation differences for sapping far greater than what has been observed in previous studies (eg: Salese et al., 2019). Other suggested sources include subsurface outflows from aquifer over-pressurization, possibly from volcanic heating, impact fracturing of overlaying units, or the raising of subsurface water tables (Andrews-Hanna et al., 2007). However, such point sources are not observed in our study region.

The lack of a localized origin can indicate a distributed source for fluvial activity. Precipitation in the form of snow or ice, with subsequent basal melting of ice deposits would leave no erosional marks until the runoff concentrated to the point of carving the observed channels. Mangold et al., (2008) described several potential sources for the channels observed to the south of our study region. Alternatively, periodic high obliquity (Laskar et al., 2004) may enable low latitude ice deposits in the region. Basal melting of such ice could provide the fluids required to carve the observed morphology and could focus the flow along specific channels. A widespread surface ice source would explain the diffuse nature of the source fluvial morphology on the volcanics and the lack of a localized source, similar to that we see with the thumbprint terrain scattered throughout the northern plains of Mars (Lockwood and Kargel, 1994). The volume of water from that source had to fill the basin above 200 m from the floor level to the −2350 m contour in order to discharge through the eastern outlet channel, following the braiding paths atop the volcanic terrain (Fig. 4A). The tributary channels suggest a distributed source, otherwise they would require multiple subsurface breakouts that would then follow separate paths. If a breakout resulted in significant discharge, it would likely concentrate in a single deep channel along the strongest topographic gradient or most mechanically susceptible rock layers. In contrast, the observed shallow, narrow channels are more consistent with minor flow volumes sourced from a wider area with regional precipitation, likely a snow or ice layer. The low branching angle of 43° ± 21° also indicate these channels were fed by the hydrological cycle. Channels fed by the hydrological cycle have an average bifurcation angle of 45° compared to groundwater sapping which has much wider bifurcation angles of 73° on average (Seybold et al., 2018).

4.2. Q2: What terminated a large volcanic flow to preserve an isolated basin?

Question 2 arises given proximity to the Syrtis volcano with widespread and low viscosity lava flows (Bandfield et al., 2000; Ehlmann and Mustard, 2012; Simpson et al., 1982) that end abruptly at the basin margin after forming a topographically flat mesa. The basin had to survive regional volcanism, erosion of the surrounding terrains, and potential lacustrine fill to remain a topographic low. Conversely, 1100 km to the south, similar small basins in the Noachian terrain have been floored by Syrtis lava flows, so how did this depression persist despite similarly expected lava flow extent? Considering the embayment relationships observed elsewhere on the margin of Syrtis Major (Fawdon, 2016), as lava advanced it should filled the basin if it encountered the modern landscape. This suggests that this location was different when the lava from Syrtis Major Planum was emplaced elsewhere. The lava flows that were halted are aged 3.4 ± 0.05 Ga. This is 1.3 Ga older than the model age for deposits on the basin floor. This suggests an obstruction that halted the volcanic flows near the irregular surface (Fig. 4E), but disappeared subsequently to allow younger lava flows to infill the basin. Previous work has shown that the thickness of the Syrtis Major volcanic flows range from 20 to 40 m (Fawdon et al., 2013; Hiesinger and Head, 2004), however, the cliffs formed at the flow terminations of the mesa are over 100 m, well outside of the measurements taken throughout Syrtis Major. While the lava should have continued to flow since the estimated critical thickness is dramatically lower than the observed cliff heights, we also find the volcanic mesa to be many meters thicker than expected and does not follow the local topography. This suggests the flows came in contact with an obstruction and caused a pooling effect at the base of the flows (Fig. 10), rather than emplacement being arrested by endogenic factors, which would create both the topographically flat area, as well as the much thicker section of volcanics.

A higher Noachian plain could have stopped abutting lava flows, and eroded subsequently to the modern basin. However, it would be mechanically unlikely for aeolian or fluvial erosion to create the basin associated with channels. Such processes can deflate surfaces or cut channels, but they commonly fill basins, not create them. Nevertheless, a depression could form through erosional processes if there was an initial heterogeneity in the Noachian material with spatially coincidental less-resistant material deflating to form the basin. That hypothesis is not testable with current satellite observations, due to resolution limits and difficulties in quantifying variations in relative ages. Alternatively, friable, yet non-lithic, material may have occupied the basin at the time of the lava flows. A simple mechanism that would fit our observations would be a >1 km thick ice sheet (Fig. 10). This would have halted lava flows (Fig. 10), and contributed the edge effects observed by Ivanov and Head (2003) that differ from volcanic flow terminations found elsewhere around Syrtis Major (Fawdon, 2016). Using numerical modeling, proposed ice sheet thickness range from 1 to 2 km within this area, in line with estimates based on the halting of the lava flows (Souček et al., 2015). The relatively thin ice sheet required for Souček et al. (2015) hypothesis, compared to adjacent areas reaching thickness as high as 5 km, further enhances its feasibility.

4.2.1. Terrestrial and Martian analogues for lava ice interactions

The Hoodoo Mountain serves as an ideal analogue to the diverse lava ice interactions that can possibly form dependent on their spatial relationship relative between the ice and lava. The Hoodoo Mountain located in Coast Mountains of British Columbia contains a multitude of varying lava ice interactions over various different eruptive cycles dependent on the location of the ice relative to the lava when erupted. One of the most prominent interactions recorded are the cliffs ranging from 50 to 200 m found at the base of the volcano (Edwards et al., 1999; Souther, 1992). This is in contrast to the origin flows which begin at thicknesses of <30 m and begin to thicken downslope as the lava is dammed and ponded by massive ice units that were >500 m in thickness (Edwards and Russell, 2002). The cliff face of the lava ice interaction is nearly covered with cooling joints with a radius of <30 cm (Edwards and Russell, 2002). While the proposed lava ice contact may have resulted in such joints at the proposed lava ice boundary of Syrtis Major, such joints are currently invisible as they would be vertical along the cliff face in addition to their expected size near the resolving limitations of the HiRISE instrument. However, this would be a testable with local visual observations by the Mars 2020 Rover.

The lateral, subaerial contacts that we infer would lack many of the distinctive characteristics of subglacial and supraglacial contacts (Edwards and Russell, 2002). Lava flows that are halted by ice and form large cliffs in the process have occurred in multiple other locations, such as the Fimmvörðuháls eruption (Edwards et al., 2012) and Clinker Mountain (Mathews, 1952) on Earth, and within Pavonis Mons (Shean et al., 2005) on Mars. In contrast, at subglacial contacts a multitude of lava domes, breccia, and exposed spines arise (Edwards and Russell, 2002). Also contrasting with lateral contacts, supraglacial contacts are marked by vesicular dome structures, similar to the ones found in subglacial contacts (Edwards and Russell, 2002), or rootless cones (Fagents and Thordarson, 2009). Accordingly, as a lateral contact, the only lava ice interaction recorded in the study area is a substantially thickened flow downslope terminating in steep cliffs as a result of the ice-dammed lava flow.

4.3. Q3: What enabled basin drainage via topographically higher outlet channels, despite the existence of a topographically lower potential outlet to the SE?

Any lake level above the −2450 m contour that completely encloses

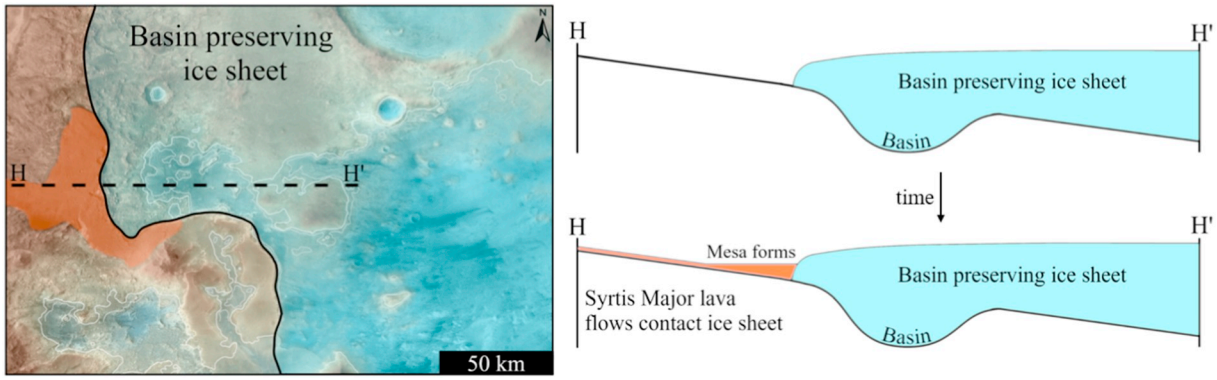

Fig. 10. Location of the basin preserving ice sheet and illustration showing formation of the topographically flat mesa due to the ice damming the flow and causing a pooling.

the current basin would cause basin discharge through southeast passage. However, the eastern outlet channel has a head elevation of −2330 m, requiring an additional 120 m of water depth. The basin shows evidence for lacustrine deposition through the equipotential filling of the magnesium carbonate layer (Fig. 7), in addition to the layered sulfate deposits with dip angles lower than 10° discussed in detail by Quinn and Ehlmann (2019). We consider three hypotheses to explain the paradox of a developed eastern outlet channel despite the gravitationally favored drainage to the southeast.

The first hypothesis to explain the existence of the eastern outlet channel is that the current landscape may not represent the topography during the time of fluvial activity. Regional or local subsidence, uplift, or rebound, possibly from an ice sheet, could have modified the local topography enough to affect the boundaries of the paleolake shore and made the southeastern gap the low point in the basin rim, instead of the eastern outlet. However, this had to happen after the emplacement of the volcanics, the time of activity for this system, and would be expected to cause significant faulting and jointing which are not observed.

A second hypothesis to explain the existence of the eastern outlet is that a continuation of the sulfate and volcanic cap unit observed to the west of the passage may have created a wall and blocked the southeastern passage. We do not observe significant fluvial erosion within this passage, although it may be obscured by the lag deposits and debris that floors the passage. However, fluvial morphology is absent even beyond the roughly ~ 3 km passage length obscured by such debris. Alternatively, landslides of sulfate and volcanic wall material could have formed a dam, followed by aeolian deflation after the fluvial activity ended, or by dam collapse during a late fluvial episode. However, given the absence of significant block, boulders, or breccia within the outlet and the surrounding area, the hypothesis of a lithic blockage is unsupported.

The third hypothesis for the existence of the eastern outlet is that ice-dams temporarily blocked flow though the southeast outlet. A ~40° obliquity occurring as recently as 5 Ma ago suggests the likelihood of glaciation at that time (Laskar et al., 2004). A mere 200 m high ice dam could block the southeast passage and force discharge through the eastern passage (Fig. 11). Regional ice units, of atmospheric provenance, would also be consistent with the evidence for a diffuse source for the fluvial activity. The ablation of the ice dam after the basin drained, evaporated, or sublimated could remove evidence of the passage blockage without leaving traces of material (Fig. 11). The observed lack of fractures and faults, lack of a debris field, and lack of erosional features in the southeast passage would best be explained by the sublimated ice dam hypothesis.

4.4. Global ocean implications

In Section 3.4 we mentioned a dissected fan that was potentially once a terminal delta at −3050 m. The relatively small and simple morphology suggests a short period of formation, or extensive resurfacing and erosion. The eroded nature of the fan precludes observations of deltaic structures such as topsets, foresets, and bottomsets and cannot uniquely distinguish between a dry alluvial fan emplacement and a submerged delta that underwent extensive erosion. The existence of additional channels down slope toward the Isidis Basin suggest multiple channel flow episodes occurring before the fan development so as not to be cut by the topographically lower channels. The channels may have once linked to the main system and might be remnants of an older, larger flow or a lower water level within Isidis. Alternatively, the channels may be independent of our system given their distance from the fan in conjunction with being separated by basin floor material.

The fan's topographic high of −3050 m approximates that of the delta located in the south of the Isidis Basin (Erkeling et al., 2012). However, the fan is located 250 m lower than the cliff forming shoreline in southern Isidis proposed by Erkeling et al., (2012) at −2800 m, and 550 m lower than the roughly −2500 m shoreline proposed by many others based on deltas (Di Achille and Hynek, 2010; Fawdon et al., 2018; Molina et al., 2017). While these observations are not supportive of a global ocean, they do not necessarily preclude it either. The existence of an ocean would not support the morphology seen in this area such as the irregular volcanic flow terminations, the preservation of this basin, and the outlet channels flowing to a topographically higher outlet than available.

4.5. Glacial implications

Large scale glaciation has been suggested in the Northeast Syrtis region previously (Bramble et al., 2017; Guidat et al., 2015; Ivanov and Head, 2003; Souček et al., 2015), which we advance with geomorphological observations revealing the possibility and extent of local ice deposits. To preserve the basin at the edge of the Syrtis Major flows, ice would need to have been present during the end stages of the Syrtis Major emplacement (Fig. 10), crater-counted to 3.4 Ga. Furthermore, while it is difficult to morphologically bound the height of ice, the basin is surrounded by coherent volcanic surfaces directly to the south that are 700 m higher than the deepest part of the basin and nearly 1 km higher to the west where source channels are present. If the Syrtis Major lava or pyroclastic flows overtopped the ice unit, a visible volcanic debris field would be expected as the ice melted away. The lack of the volcanic debris field suggests that the ice sheet would have been at least 1 km thick when the current flow front formed, also consistent with numerical models which put the thickness of the potential ice sheet above this limit (Souček et al., 2015). There is a lack of classic glacial landforms such as ribbed moraines in the case of a wet-based glacier or cold-based subglacial meltwater channels in the immediate study area, but such assemblages are usually located at the base of the ice. While this study area

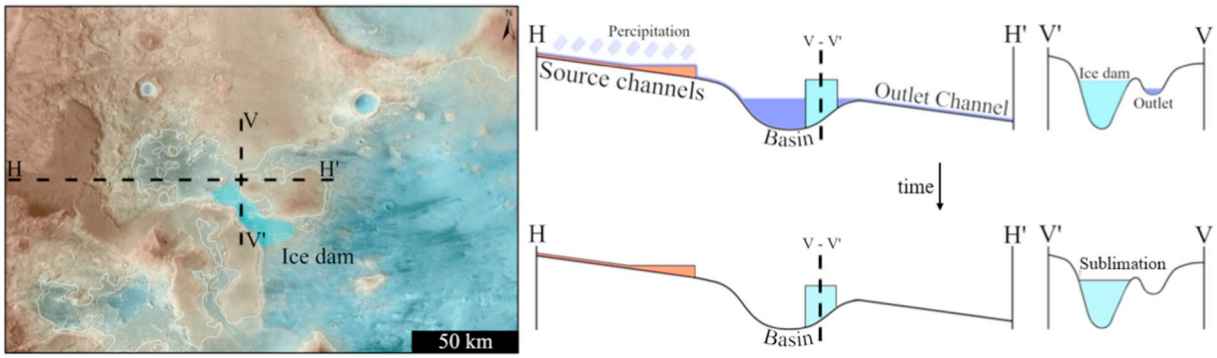

Fig. 11. Location of the ice dam causing a blockage to the southeastern outlet of the basin along with an illustration showing the timeline of the inlet and outlet channel formation followed by the sublimation of the ice dam. The ice dam schematic is the minimum amount of ice required to match the observations, and actual ice coverage may have exceeded this amount by many factors.

lacks such commonly expected morphologies associated with glacial landforms, it is still modeled to have been covered by an Isidis Basin ice sheet (Souček et al., 2015). Additionally, there are multiple glacial features mapped throughout the surrounding area (Guidat et al., 2015), along with many areas that lack these features, even though all are modeled to have been covered by an ice sheet (Souček et al., 2015). The abundant glacial features mapped have been dated to 3.4–3.1 Ga (Guidat et al., 2015; Ivanov et al., 2012), which coincides with the time period of an Isidis ice sheet based on modeling of 3.4–2.8 Ga (Souček et al., 2015), in addition to the volcanics that were dammed and ponded to form the topographically flat mesa, dated to 3.4 ± 0.05 Ga (Figs. 9A, 10). The existence of this ice sheet, and the associated morphologies, all coincide with the halted Syrtis Major lava flow of the same age. While it is possible the ice sheet existed before or after the mentioned time period, current observations do not constrain the secular direction.

The observed fluvial geomorphology and multiple outflow channels suggest multiple episodes of drainage based upon the multiple paths taken by the channels. That is consistent with climate cycles that episodically emplace regional ice with some basal melting. The outlet channels are too small to retain craters for accurate chronology. Higher resolution data would be needed to better resolve the number, duration, and possibly order of glacial episodes in their relation to the outlet channels. However, the most complex portion of the outlet channels show three parallel sections (Fig. 6). If each drainage episode created a separate channel section, and a final episode drained through the modern southeastern break in the basin, a minimum of four discharge events are expected. It is likely that channels sustained multiple, temporally separated, flows and that evidence of early events would have been resurfaced or eroded by later ones. This leaves open the possibility of a multitude of fluvial episodes that mirror climate cycles tied to the proposed glacio-fluvial basin.

5. Conclusions

The Hesperian-aged fluvial system located on the northeast Syrtis boundary records important late stage geologic events that are vital to understanding the region's history. Our observations and interpretations collectively contribute to the understanding of the glaciofluvial processes in the northeast Syrtis region. We consider a second distinct episode of fluvial activity in the region, following the first associated with the Jezero open basin crater lake at 3.74 Ga (Fassett and Head, 2008). Our observations establish that this second episode occurred after the early Hesperian emplacement of Syrtis Major volcanics. The fluvial system is defined by high elevation upland source channels on the western basalts (Bandfield et al., 2000) that indicate the system's source, a topographic basin that indicates fluvial storage, and an outlet channel flowing toward the low elevation Isidis Basin. The diffuse source morphology and low branching angles suggest an atmospheric origin of the system's water. The basin is preserved at the base of Syrtis Major, juxtaposed by low viscosity lava rheology that terminates in high cliffs, consistent with a basin-wide ice sheet that was at least 1 km thick. The well-developed outlet channel is gravitationally disfavored and would require either significant obliteration of flow features on the gravitationally favored southeast edge of the basin or a temporary paleo ice dam preventing such discharge, further illuminating the glacio-fluvial history of the region. Future local observations by the Mars 2020 Rover, particularly of structural geology along the cliff face abutting the basin, would help test our interpreted glaciofluvial history of this region.

Acknowledgments

This work has benefited from reviews and discussions with Tim Goudge, Steven Ruff, Jim Head, and Bethany Ehlmann. We thank Caleb Fassett for providing the CTX DEM processing of the outlet fan and Tim Goudge for providing the basin Depression CTX DEM. All data and observations used in this study are publically available from the NASA PDS. Derived products such as produced CTX DEMs can be attained through processing or via archived content at the Planetary Science Lab web page and LSU's Digital Commons. Connor Matherne was supported by the Frank's Chair funds, W.L. Calvert Memorial Scholarship, NASA-EPSCoR funded LASpace Graduate Student Research Assistantship grant, and Louisiana Board of Regents Research Award Program grant LEQSF-EPS(2017)-RAP-22 awarded to Karunatillake. J.R. Skok was supported with the MDAP award NNX14AR93G. Suniti Karunatillake's work was supported by NASA-MDAP grant 80NSSC18K1375.

References

Andrews-Hanna, J.C., Lewis, K.W., 2011. Early Mars hydrology: 2. Hydrological evolution in the Noachian and Hesperian epochs. J. Geophys. Res. E: Planets 116, 1–20. https://doi.org/10.1029/2010JE003709.

Andrews-Hanna, J.C., Phillips, R.J., Zuber, M.T., 2007. Meridiani Planum and the global hydrology of Mars. Nature 446, 163–166. https://doi.org/10.1038/nature05594.

Bandfield, J.L., Hamilton, V.E., Christensen, P.R., 2000. A global view of Martian surface compositions from MGS-TES. Science 287, 1626–1630. https://doi.org/10.1126/science.287.5458.1626 (80-.).

Bibring, J.P., Langevin, Y., Mustard, J.F., Poulet, F., Arvidson, Raymond, Gendrin, A., Gondet, B., Mangold, N., Pinet, P., Forget, F., Berthe, M., Gomez, C., Jouglet, D., Soufflot, A., Vincendon, M., Combes, M., Drossart, P., Encrenaz, T., Fouchet, T., Merchiorri, R., Belluci, G.C., Altieri, F., Formisano, V., Capaccioni, F., Cerroni, P., Coradini, A., Fonti, S., Korablev, O., Kottsov, V., Ignatiev, N., Moroz, V., Titov, D., Zasova, L., Loiseau, D., Pinet, Patrick, Douté, S., Schmitt, B., Sotin, C., Hauber, E., Hoffmann, H., Jaumann, R., Keller, U., Arvidson, Ray, Duxbury, T., Forget, François, Neukum, G., 2006. Global mineralogical and aqueous Mars history derived from OMEGA/Mars express data. Science (80-.) 312, 400–404. https://doi.org/10.1126/science.1122659.

Bramble, M.S., Mustard, J.F., Salvatore, M.R., 2017. The geological history of Northeast Syrtis Major, Mars. Icarus 293, 66–93. https://doi.org/10.1016/j.icarus.2017.03.030.

Crown, D.A., Ramsey, M.S., 2017. Morphologic and thermophysical characteristics of lava flows southwest of Arsia Mons, Mars. J. Volcanol. Geotherm. Res. 342, 13–28. https://doi.org/10.1016/j.jvolgeores.2016.07.008.

Davila, A.F., Fairén, A.G., Stokes, C.R., Platz, T., Rodriguez, A.P., Lacelle, D., Dohm, J., Pollard, W., 2013. Evidence for Hesperian glaciation along the Martian dichotomy boundary. Geology 41, 755–758. https://doi.org/10.1130/G34201.1.

Di Achille, G., Hynek, B.M., 2010. Ancient ocean on Mars supported by global distribution of deltas and valleys. Nat. Geosci. 3, 459–463. https://doi.org/10.1038/ngeo891.

Dickson, J.L., Kerber, L., Fassett, C.I., Ehlmann, B.L., 2018. A global, blended CTX mosaic of Mars with vecotrized seam mapping: a new mosaicking pipeline using principles of non-destructive image editing. In: 49th Lunar and Planetary Science Conference 2018. https://doi.org/10.1590/s1809-98232013000400007.

Edwards, L., Broxton, M., 2012. Automated 3D surface reconstruction from orbital imagery. Lunar planet. Sci. Conf 39. https://doi.org/10.2514/6.2006-7435 (01461, 2419).

Edwards, B.R., Russell, J.K., 2002. Glacial influences on morphology and eruptive products of Hoodoo Mountain volcano, Canada. Geol. Soc. Lond. Spec. Publ. 202, 179–194.

Edwards, B.R., Anderson, R.G., Russell, J.K., Hastings, N.L., Guo, Y.T., 1999. The Quaternary Hoodoo Mountain Volcanic Complex and Paleozoic and Mesozoic Basement Rocks: Parts of Hoodoo Mountain (NTS 104B/14) and Craig River (NTS 104B/11) Map Areas, Northwestern British Columbia. Geological Survey of Canada.

Edwards, B., Magnússon, E., Thordarson, T., Gumundsson, M.T., Höskuldsson, A., Oddsson, B., Haklar, J., 2012. Interactions between lava and snow/ice during the 2010 Fimmvö ruháls eruption, South-Central Iceland. J. Geophys. Res. Solid Earth 117, 1–21. https://doi.org/10.1029/2011JB008985.

Edwards, B.R., Karson, J., Wysocki, R., Lev, E., Bindeman, I., Kueppers, U., 2013. Insights on lava-ice/snow interactions from large-scale basaltic melt experiments. Geology 41, 851–854. https://doi.org/10.1130/G34305.1.

Ehlmann, B.L., Mustard, J.F., 2012. An in-situ record of major environmental transitions on early Mars at Northeast Syrtis Major. Geophys. Res. Lett. 39 https://doi.org/10.1029/2012GL051594.

Ehlmann, B.L., Mustard, J.F., Fassett, C.I., Schon, S.C., Head, J.W., Des Marais, D.J., Grant, J.A., Murchie, S.L., 2008. Clay minerals in delta deposits and organic preservation potential on Mars. Nat. Geosci. 1, 355–358. https://doi.org/10.1038/ngeo207.

Ehlmann, B.L., Mustard, J.F., Murchie, S.L., Poulet, F., Bishop, J.L., Brown, A.J., Calvin, W.M., Clark, R.N., Marais, D.J.D., Milliken, R.E., Roach, L.H., Roush, T.L., Swayze, G.A., Wray, J.J., 2008. Orbital identification of carbonate-bearing rocks on Mars. Science 322, 1828–1832. https://doi.org/10.1126/science.1164759 (80-.).

Ehlmann, B.L., Mustard, J.F., Swayze, G.A., Clark, R.N., Bishop, J.L., Poulet, F., Des Marais, D.J., Roach, L.H., Milliken, R.E., Wray, J.J., Barnouin-Jha, O., Murchie, S.L., 2009. Identification of hydrated silicate minerals on Mars using MRO-CRISM: geologic context near Nili Fossae and implications for aqueous alteration. J. Geophys. Res. E Planets 114. https://doi.org/10.1029/2009JE003339.

Erkeling, G., Reiss, D., Hiesinger, H., Poulet, F., Carter, J., Ivanov, M.A., Hauber, E., Jaumann, R., 2012. Valleys, paleolakes and possible shorelines at the Libya Montes/

Isidis boundary: implications for the hydrologic evolution of Mars. Icarus 219, 393–413. https://doi.org/10.1016/j.icarus.2012.03.012.
Fagents, S.A., Thordarson, T., 2009. Rootless volcanic cones in Iceland and on Mars. Geol. Mars 151–177. https://doi.org/10.1017/cbo9780511536014.007.
Fassett, C.I., Head, J.W., 2005. Fluvial sedimentary deposits on Mars: ancient deltas in a crater lake in the Nili Fossae region. Geophys. Res. Lett. 32, 1–5. https://doi.org/10.1029/2005GL023456.
Fassett, C.I., Head, J.W., 2008. The timing of Martian valley network activity: constraints from buffered crater counting. Icarus 195, 61–89. https://doi.org/10.1016/j.icarus.2007.12.009.
Fawdon, P., 2016. The Volcanic Evolution of Syrtis Major Planum, Mars.
Fawdon, P., Balme, M.R., Vye-Brown, C., Rothery, D.A., Jordan, C.J., 2013. The evolution of volcanism in Syrtis Major planum (Mars): drawing insight from terrestrial analogues. Lunar Planet. Sci. Conf. 44, 6–7.
Fawdon, P., Gupta, S., Davis, J.M., Warner, N.H., Adler, J.B., Balme, M.R., Bell, J.F., Grindrod, P.M., Sefton-Nash, E., 2018. The Hypanis Valles delta: the last highstand of a sea on early Mars? Earth Planet. Sci. Lett. 500, 225–241. https://doi.org/10.1016/j.epsl.2018.07.040.
Fawdon, P., Balme, M.R., Vye-Brown, C., Jordan, C.J., Rothery, D.A., 2019. The age of Syrtis Major Planum and implications for the Circum-Isidis region. In: Lunar and Planetary Science Conference.
Fergason, R.L, Hare, T.M., Laura, J., 2018. HRSC and MOLA Blended Digital Elevation Model at 200m v2, Astrogeology PDS Annex. U.S. Geological Survey. http://bit.ly/HRSC_MOLA_Blend_v0.
Goudge, T.A., Mustard, J.F., Head, J.W., Fassett, C.I., 2012. Constraints on the history of open-basin lakes on Mars from the composition and timing of volcanic resurfacing. J. Geophys. Res. E Planets 117. https://doi.org/10.1029/2012JE004115.
Goudge, T.A., Mustard, J.F., Head, J.W., Fassett, C.I., Wiseman, S.M., 2015. Assessing the mineralogy of the watershed and fan deposits of the Jezero crater paleolake system, Mars. J. Geophys. Res. Planets 120, 775–808. https://doi.org/10.1002/2014JE004782.
Guidat, T., Pochat, S., Bourgeois, O., Souček, O., 2015. Landform assemblage in Isidis Planitia, Mars: evidence for a 3 Ga old polythermal ice sheet. Earth Planet. Sci. Lett. 411, 253–267. https://doi.org/10.1016/j.epsl.2014.12.002.
Hartmann, W.K., 2005. Martian cratering 8: Isochron refinement and the chronology of Mars. Icarus 174, 294–320. https://doi.org/10.1016/j.icarus.2004.11.023.
Hiesinger, H., Head, J.W., 2004. The Syrtis Major volcanic province, Mars: Synthesis from Mars global surveyor data. J. Geophys. Res. 109. https://doi.org/10.1029/2003je002143.
Hirt, C., Claessens, S.J., Kuhn, M., Featherstone, W.E., 2012. Kilometer-resolution gravity field of Mars: MGM2011. Planet. Space Sci. 67, 147–154. https://doi.org/10.1016/j.pss.2012.02.006.
Ivanov, M.A., Head III, J.W., 2003. Syrtis Major and Isidis Basin contact: morphological and topographic characteristics of Syrtis Major lava flows and material of the Vastitas Borealis Formation. J. Geophys. Res. Planets 108 (E6). https://agupubs.onlinelibrary.wiley.com/doi/full/10.1029/2002JE001994.
Ivanov, M.A., Hiesinger, H., Erkeling, G., Hielscher, F.J., Reiss, D., 2012. Major episodes of geologic history of Isidis Planitia on Mars. Icarus 218, 24–46. https://doi.org/10.1016/j.icarus.2011.11.029.
Laskar, J., Correia, A.C.M., Gastineau, M., Joutel, F., Levrard, B., Robutel, P., 2004. Long term evolution and chaotic diffusion of the insolation quantities of Mars. Icarus 170, 343–364. https://doi.org/10.1016/j.icarus.2004.04.005.
Lockwood, J., Kargel, J., 1994. Thumbprint terrain in Isidis Planitia: Formed in a glacial Paleolake environment. In: Lunar and Planetary Institute Science, p. 799.
Malin, M.C., Bell, J.F., Cantor, B.A., Caplinger, M.A., Calvin, W.M., Clancy, R.T., Edgett, K.S., Edwards, L., Haberle, R.M., James, P.B., Lee, S.W., Ravine, M.A., Thomas, P.C., Wolff, M.J., 2007. Context camera investigation on board the Mars reconnaissance orbiter. J. Geophys. Res. E Planets 112. https://doi.org/10.1029/2006JE002808.
Mangold, N., Ansan, V., Baratoux, D., Costard, F., Dupeyrat, L., Hiesinger, H., Masson, P., Neukum, G., Pinet, P., 2008. Identification of a new outflow channel on Mars in Syrtis Major Planum using HRSC/MEx data. Planet. Space Sci. 56, 1030–1042. https://doi.org/10.1016/j.pss.2008.01.011.
Mathews, W.H., 1952. Ice-dammed lavas from Clinker Mountain, southwestern British Columbia. Am. J. Sci. https://doi.org/10.2475/ajs.250.8.553.
McEwen, A.S., Preblich, B.S., Turtle, E.P., Artemieva, N.A., Golombek, M.P., Hurst, M., Kirk, R.L., Burr, D.M., Christensen, P.R., 2005. The rayed crater Zunil and interpretations of small impact craters on Mars. Icarus 176, 351–381. https://doi.org/10.1016/j.icarus.2005.02.009.
McEwen, A.S., Eliason, E.M., Bergstrom, J.W., Bridges, N.T., Hansen, C.J., Delamere, W.A., Grant, J.A., Gulick, V.C., Herkenhoff, K.E., Keszthelyi, L., kirk, R.L., Mellon, M.T., Squyres, S.W., Thomas, N., Weitz, C.M., 2007. Mars reconnaissance orbiter's high resolution imaging science experiment (HiRISE). J. Geophys. Res. E Planets 112. https://doi.org/10.1029/2005JE002605.
McGuire, P.C., Bishop, J.L., Brown, A.J., Fraeman, A.A., Marzo, G.A., Frank Morgan, M., Murchie, S.L., Mustard, J.F., Parente, M., Pelkey, S.M., Roush, T.L., Seelos, F.P., Smith, M.D., Wendt, L., Wolff, M.J., 2009. An improvement to the volcano-scan algorithm for atmospheric correction of CRISM and OMEGA spectral data. Planet. Space Sci. 57, 809–815. https://doi.org/10.1016/j.pss.2009.03.007.
Molina, A., López, I., Prieto-Ballesteros, O., Fernández-Remolar, D., de Pablo, M., Gómez, F., 2017. Coogoon Valles, western Arabia Terra: hydrological evolution of a complex Martian channel system. Icarus 293, 27–44. https://doi.org/10.1016/j.icarus.2017.04.002.
Murchie, S., Arvidson, R., Bedini, P., Beisser, K., Bibring, J.P., Bishop, J., Boldt, J., Cavender, P., Choo, T., Clancy, R.T., Darlington, E.H., Des Marais, D., Espiritu, R., Fort, D., Green, R., Guinness, E., Hayes, J., Hash, C., Heffernan, K., Hemmler, J., Heyler, G., Humm, D., Hutcheson, J., Izenberg, N., Lee, R., Lees, J., Lohr, D., Malaret, E., Martin, T., McGovern, J.A., McGuire, P., Morris, R., Mustard, J., Pelkey, S., Rhodes, E., Robinson, M., Roush, T., Schaefer, E., Seagrave, G., Seelos, F., Silverglate, P., Slavney, S., Smith, M., Shyong, W.J., Strohbehn, K., Taylor, H., Thompson, P., Tossman, B., Wirzburger, M., Wolff, M., 2007. Compact Connaissance Imaging Spectrometer for Mars (CRISM) on Mars Reconnaissance Orbiter (MRO). J. Geophys. Res. E Planets 112. https://doi.org/10.1029/2006JE002682.
Mustard, J.F., Cooper, C.D., Rifkin, M.K., 2001. Evidence for recent climate change on Mars from the identification of youthful near-surface ground ice. Nature 412, 411–414. https://doi.org/10.1038/35086515.
Mustard, J.F., Poulet, F., Head, J.W., Mangold, N., Bibring, J.P., Pelkey, S.M., Fassett, C.I., Langevin, Y., Neukum, G., 2007. Mineralogy of the Nili fossae region with OMEGA/Mars express data: 1. Ancient impact melt in the Isidis Basin and implications for the transition from the Noachian to Hesperian. J. Geophys. Res. E Planets 112. https://doi.org/10.1029/2006JE002834.
Mustard, J.F., Ehlmann, B.L., Murchie, S.L., Poulet, F., Mangold, N., Head, J.W., Bibring, J.P., Roach, L.H., 2009. Composition, morphology, and stratigraphy of Noachian crust around the Isidis basin. J. Geophys. Res. E Planets 114. https://doi.org/10.1029/2009JE003349.
Neukum, G., Jaumann, R., 2004. HRSC: the high resolution stereo camera of Mars express, in: Mars Express: The Scientific Payload. Mars Express Sci. Payload. Ed. by Andrew Wilson 1–19.
Palumbo, A.M., Head, J.W., 2018. Impact cratering as a cause of climate change, surface alteration, and resurfacing during the early history of Mars. Meteorit. Planet. Sci. 53, 687–725. https://doi.org/10.1111/maps.13001.
Quinn, D.P.P., Ehlmann, B.L.L., 2019. The deposition and alteration history of the northeast Syrtis layered sulfates. J. Geophys. Res. Planets. https://doi.org/10.1029/2018je005706.
Rogers, A.D., Warner, N.H., Golombek, M.P., Head, J.W., Cowart, J.C., 2018. Areally extensive surface bedrock exposures on Mars: many are clastic rocks, not lavas. Geophys. Res. Lett. 45, 1767–1777. https://doi.org/10.1002/2018GL077030.
Rothery, D.A., McBride, N., Gilmour, I., 2018. An Introduction to the Solar System. Cambridge University Press.
Salese, F., Pondrelli, M., Neeseman, A., Schmidt, G., Ori, G.G., 2019. Geological evidence of planet-wide groundwater system on Mars. J. Geophys. Res. Planets. https://doi.org/10.1029/2018JE005802.
Schaber, G.G., 2008. Syrtis major: a low-relief volcanic shield. J. Geophys. Res. 87, 9852. https://doi.org/10.1029/jb087ib12p09852.
Schon, S.C., Head, J.W., Fassett, C.I., 2012. An overfilled lacustrine system and progradational delta in Jezero crater, Mars: implications for Noachian climate. Planet. Space Sci. 67, 28–45. https://doi.org/10.1016/j.pss.2012.02.003.
Seybold, H., Rothman, D.H., Kirchner, J.W., 2017. Climate's watermark in the geometry of stream networks. Geophys. Res. Lett. 44, 2272–2280. https://doi.org/10.1002/2016GL072089.
Seybold, H.J., Kite, E., Kirchner, J.W., 2018. Branching geometry of valley networks on mars and earth and its implications for early Martian climate. Sci. Adv. 4, 1–6. https://doi.org/10.1126/sciadv.aar6692.
Shean, D.E., Head, J.W., Marchant, D.R., 2005. Origin and evolution of a cold-based tropical mountain glacier on Mars: the Pavonis Mons fan-shaped deposit. J. Geophys. Res. E: Planets 110, 1–35. https://doi.org/10.1029/2004JE002360.
Simpson, R.A., Tyler, G.L., Harmon, J.K., Peterfreund, A.R., 1982. Radar measurement of small-scale surface texture: Syrtis major. Icarus 49, 258–283. https://doi.org/10.1016/0019-1035(82)90076-8.
Souček, O., Bourgeois, O., Pochat, S., Guidat, T., 2015. A 3 Ga old polythermal ice sheet in Isidis Planitia, Mars: dynamics and thermal regime inferred from numerical modeling. Earth Planet. Sci. Lett. 426, 176–190. https://doi.org/10.1016/j.epsl.2015.06.038.
Souther, J.G., 1992. The Late Cenozoic Mount Edziza Volcanic Complex, British Columbia. Geological Survey of Canada.
Stolper, E., Walker, D., 1980. Melt density and the average composition of basalt. Contrib. Mineral. Petrol. 74, 7–12. https://doi.org/10.1007/BF00375484.
Susko, D., Karunatillake, S., Kodikara, G., Skok, J.R., Wray, J., Heldmann, J., Cousin, A., Judice, T., 2017. A record of igneous evolution in Elysium, a major Martian volcanic province. Sci. Rep. 7, 43177 https://doi.org/10.1038/srep43177.
Tornabene, L.L., Moersch, J.E., McSween, H.Y., Hamilton, V.E., Piatek, J.L., Christensen, P.R., 2008. Surface and crater-exposed lithologic units of the Isidis based as mapped by coanalysis of THEMIS and TES derived data products. J. Geophys. Res. E Planets 113. https://doi.org/10.1029/2007JE002988.
Warner, N.H., Gupta, S., Calef, F., Grindrod, P., Boll, N., Goddard, K., 2015. Minimum effective area for high resolution crater counting of Martian terrains. Icarus 245, 198–240. https://doi.org/10.1016/j.icarus.2014.09.024.
Werner, S.C., 2008. The early Martian evolution-constraints from basin formation ages. Icarus 195, 45–60. https://doi.org/10.1016/j.icarus.2007.12.008.
Wichman, R.W., Schultz, P.H., 2008. Sequence and mechanisms of deformation around the Hellas and Isidis impact basins on Mars. J. Geophys. Res. 94, 17333. https://doi.org/10.1029/jb094ib12p17333.
Wilson, L., Head, J.W., 1994. Review and analysis of volcanic eruption to theory relationships landforms. Rev. Geophys. 32, 221–263.
Zuber, M.T., 1992. The Mars observer laser altimeter investigation. J. Geophys. Res. 97, 7781–7797. https://doi.org/10.1029/92JE00341.